Paper No.
10990

NACE INTERNATIONAL CORROSION 2018 Conference & Expo

Effect of Pyrrhotite on Mild Steel Corrosion in Aqueous CO_2 and H_2S Solutions

Saba Navabzadeh Esmaeely, Gheorghe Bota, Bruce Brown, Srdjan Nesic
Institute for Corrosion and Multiphase Flow Technology, Department of Chemical and Biomolecular Engineering, Ohio University, Athens, OH 45701, United States

ABSTRACT

Due to the electrical conductivity of pyrrhotite it was hypothesized that its presence in the corrosion product layer on a steel surface could lead to localized corrosion. Mild steel specimens (API 5L X65) were pretreated to form a pyrrhotite layer on the surface using high temperature sulfidation in oil. The pretreated specimens were then exposed to a range of aqueous CO_2 and H_2S corrosion environments at 30 and 60°C. X-ray diffraction data showed that the pyrrhotite layer changed during exposure; in an aqueous CO_2 solution it underwent dissolution while in a mixed CO_2/H_2S solution it partially transformed to troilite, with some mackinawite formation. This led to initiation of localized corrosion in both cases. Propagation of the localized attack was enhanced due to a galvanic coupling between the pyrrhotite layer and the steel surface. The intensity of the observed localized corrosion varied with solution conductivity (NaCl concentration); a more conductive solution resulted in higher localized corrosion rates consistent with the galvanic nature of the attack propagation.

Key words: Pyrrhotite, H_2S corrosion, CO_2, localized corrosion, troilite, XRD

INTRODUCTION

In H_2S containing environments encountered in the oil and gas industry, localized corrosion is a potential cause leading to facility failure. There can be a high rate of metal loss in a very limited area, which may be covered by a corrosion product layer. This makes H_2S localized corrosion more difficult to predict and detect prior to failure by using the conventional corrosion inspection and monitoring methods.[1,2] Considering the often random spatial distribution of localized attack and the limited number of monitoring probes that can be installed in any given facility, the chances of detecting localized corrosion this way are slim at best. Internal line inspection techniques which could theoretically detect localized attack are complicated, expensive and therefore are used infrequently. Thus, a better understanding of localized corrosion mechanisms would be essential for the development of predictive models and implementation of corrosion mitigation strategies.

There are complicating factors associated with the investigation of H_2S corrosion mechanisms. This includes the recently found electrochemical mechanisms involving direct reduction of H_2S at the metal surface [3–5] and the role of different iron sulfides [6–12] that can form on the metal surface in the corrosion process. In H_2S solutions, the corrosion product layer can be composed of various iron sulfides with

distinct physicochemical and electrical properties [13–18]. The electrical conductivity of various iron sulfides is one of the key parameters. For example, pyrrhotite ($Fe_{1-x}S$), troilite (FeS) and pyrite (FeS_2) all occur as stable corrosion products and have similar electrical conductivities[13–15] while for the more unstable mackinawite (FeS) there are far fewer values reported for its conductivity[19]. Mackinawite has anisotropic electrical properties, being conductive in the direction of oriented layers in its crystal structure and much less conductive in the perpendicular direction [19]. The existence of conductive phases on a steel surface significantly impacts the electrochemically driven corrosion process [3,20,21]. The conductive corrosion product layer may intensify the electrochemical reaction rate through providing a larger cathodic surface area, locally or uniformly across the corroding steel surface.

Localized H_2S corrosion in electrolytes, typically an aqueous NaCl solution, has been attributed to three main reasons: the presence of elemental sulfur[22–25] partial formation/failure of the iron sulfide corrosion product layer [26], and formation of multiple iron sulfide polymorphs in a corrosion product layer, leading to non-uniform electrical conductivity[27–29]. Over the past decade, the role of conductive iron sulfides on localized corrosion in H_2S saturated aqueous solutions has become a focus area for corrosion scientists[27–32]. However, the research, has not yielded decisive insights into the mechanisms and the possible role of different conductive iron sulfides[27–29].

Several studies on corrosion of mild steel in H_2S/CO_2 gas mixtures have been conducted where experiments involved investigation of multiple parameters including the effect of pH and glycol[28,32–38]. In a recent study, Kvarekvål, *et al.*, [28] reported intensified uniform and localized corrosion rates under a pyrrhotite/troilite layer in the presence of a conductive electrolyte. However, due to the complexity of their experimental conditions, the corrosion mechanisms related to the observed localized corrosion remained unclear.

As for the role of conductive corrosion product layers on localized corrosion, Ning, *et al.,*[27] demonstrated that a mild steel surface could undergo localized corrosion when in direct contact with pyrite, in the presence of a corrosive electrolyte. They proposed that localized corrosion takes place as a result of galvanic coupling between pyrite and the steel. This was attributed to pyrite being conductive, hence forming a galvanic cell with the exposed part of the steel surface. However, the authors did not report localized corrosion in the presence of pyrrhotite/troilite. Considering that pyrrhotite/troilite are in a similar conductivity range as pyrite, one can expect that they could also act as a driving force for localized corrosion[13–15] (Table 1). Furthermore, they all have a similar open circuit potential (OCP), much more positive than mild steel[39–41] (Table 1). Hypothetically, when in contact with a mild steel surface, all of them could act as a cathode and lead to an increase in the corrosion rate through a galvanic effect [42].

There are earlier studies that addressed this problem. Adam, *et al.*[43] investigated the galvanic coupling of pyrrhotite with various steels and reported a larger potential difference and a higher current between the pyrrhotite and mild steel as compared to other types of galvanic couples. The authors reported a higher galvanic current at lower pH where the mild steel is not passivated. Pyrrhotite [44] and pyrite [45] are reported to be good electro-catalysts for the hydrogen evolution reaction. Thus, it appears that if the steel is coupled with one or both of these iron sulfides in a conductive acidic media, higher corrosion rates would be observed, either locally or uniformly due to an increase in cathodic surface area.[46]

Table 1
Iron sulfide properties

Material	Resistivity [13–15]	OCP in a deoxygenated solution at pH 4.0 vs. sat. Ag/AgCl [39–41]
Mild steel	≤ 10^{-8} Ωm	from **-** 0.65 to - 0.7 V
Pyrite	10^{-5} - 10 Ωm	from + 0.16 to - 0.22 V
Pyrrhotite	10^{-6} - 0.1 Ωm	from - 0.08 to - 0.22 V
Troilite	10^{-6} - 0.1 Ωm	

While there seem to be evidence of the role of pyrite in localized corrosion,[27] contradictory reports are found with respect to the role of pyrrhotite/troilite[27,28] what motivated the current study. Here, the focus is on galvanic coupling of a pyrrhotite/troilite layer with the steel underneath. Initial experiments were conducted in an aqueous electrolyte saturated with CO_2 followed by experiments in an H_2S saturated electrolyte and finally a mixed CO_2/H_2S electrolyte was used. The experiments in an aqueous CO_2 solution were conducted first, for several reasons: (i) they are much simpler and provide a good training opportunity where most of the experimental problems and analyses could be worked out before moving the experimentation into an H_2S environment which is much more challenging; (ii) the galvanic coupling between the pyrrhotite layer and the steel surface was present in both environments; and (iii) in order to study the behavior in a mixed CO_2/H_2S environment which is most realistic for field applications, it was beneficial to work with "pure" environments first. Ultimately this approach provided valuable insights into the behavior of pyrrhotite on the steel surface and enabled us to decipher the complicated interactions between the steel, the pyrrhotite layer and the corrosive environment.

EXPERIMENTAL PROCEDURE

Experimental Setup (Electrochemical Measurements)

Electrochemical experiments were conducted in a conventional three-electrode glass cell, following the experimental matrix described in Table 2. In this setup, the cell was filled with 2 liters of deionized (DI) water and 20.2 g of sodium chloride (NaCl) to obtain a 1.0 wt% NaCl electrolyte. The temperature was maintained at 30°C. Electrochemical measurements were conducted with a three-electrode setup, where a pretreated disc electrode made of X65 pipeline steel with a pyrrhotite layer, served as the working electrode (WE). A 20 mm × 30 mm platinum mesh was used as counter electrode (CE). A saturated silver/silver chloride (Ag/AgCl) reference electrode (RE) was connected *via* a salt bridge with a Luggin capillary. In addition to the steel WE, four small square steel specimens with a surface area of 3.4 cm^2 were included in the cell for the purpose of surface analysis. The H_2S gas concentration was maintained using gas rotameters and the accuracy of the concentration was confirmed by employing a gas sample pump with colorimetric H_2S detector tubes. The gas outlet was scrubbed using a 5 M sodium hydroxide solution (NaOH) and several dry carbon scrubbers to capture the H_2S.

Prior to each experiment, the electrolyte was deoxygenated by sparging with either N_2 or CO_2 gas for at least 3 hours prior to the addition of H_2S gas. The H_2S was introduced into the experimental cell at the desired concentration for at least one hour prior to immersing of the specimens, in order to ensure that the electrolyte was in equilibrium with respect to aqueous H_2S. The electrolyte was stirred at 200 rpm with a 12.7 mm stir bar to ensure proper mixing. The solution pH was adjusted to the desired value by adding a deoxygenated 1 M hydrochloric acid (HCl) or NaOH solution. Then, the X65 specimens were inserted into the glass cell.

The corrosion processes were monitored *via* open circuit potential (OCP), linear polarization resistance (LPR), and electrochemical impedance spectroscopy (EIS) measurements. The measured polarization

resistance (R_p) obtained from LPR was corrected for ohmic drop using the solution resistance (R_s) measured by EIS. The Tafel slopes used to calculate the corrosion rate from the R_p values were: –0.12 V per decade for the cathodic reaction and 0.04 V per decade for the anodic reaction. Similar Tafel slopes were reported by Zheng *et al.* [3–5] and Esmaeely *et al.*[47] in the presence of H_2S across different experimental conditions at different pH. The abovementioned authors have explicitly identified that the Tafel slope for direct reduction of H_2S was also approximately – 0.12 V per decade.

Specimen Pretreatment (Pyrrhotite Layer Generation)

In order to study the effect of the pyrrhotite layer on localized corrosion, the X65 steel specimens were "pretreated" in a different experimental setup, used to develop a reproducible pyrrhotite layer prior to their immersion into the electrochemical glass cell described above. [48,49]
In high temperature sulfidation of steel in crude oil fractions seen in refinery conditions pyrrhotite is most often found as a corrosion product. Such pyrrhotite is the same compound as seen in aqueous corrosion of steel in the presence of H_2S. It was assumed that the preformed pyrrhotite layer, which was formed ex-situ has the same properties as a pyrrhotite that forms as a corrosion product layer in aqueous H_2S environments (in-situ formation). Specimen pretreatment, which was used to form a pyrrhotite layer on the steel surface, was performed in a 1 L Inconel autoclave. A mineral oil with a sulfur content of 0.25 (wt%) was used to form the pyrrhotite layer on the steel surfaces. The autoclave has a magnetic stirrer that drives an internal impeller that homogenizes the pretreatment fluid and ensures good heat transfer.

Pyrrhotite Layer Surface Analysis

The morphology of the corrosion product layer was analyzed utilizing a scanning electron microscopy. Compositional analyses were carried out using an X-Ray diffractometer. A profilometer was used to measure pit depth.

Table 2
Test Matrix

Parameters	Conditions
Total pressure	0.1 MPa
Temperature	30, 60°C
Solution	0 and 1 wt% NaCl
Flow condition	Agitated, 200 rpm, 12.7 mm stir bar
Material	X65 with Pyrrhotite Layer
Corrosion measurement methods	LPR, EIS, and weight loss
pH_2S in the gas phase	0, 0.01 MPa in N_2 or CO_2
H_2S concentration in the liquid phase	9.3×10^{-3} molL^{-1} at 30˚C 5.5×10^{-3} molL^{-1} at 60˚C
pH	4.0, 6.2 (± 0.1)

RESULTS AND DISCUSSION

A detailed discussion of the experimental results will follow the review of characterization data for the pretreated specimens.

Pretreated Specimens

Figure 1 shows the SEM image of the corroded (top) surface and cross-section image of the pretreated specimens. In Figure 1 (a) one can see that there are two layers, a loose layer on top of a more compact

layer underneath, each has a similar gross morphology; the visual difference between the upper and lower layer is associated with delamination phenomena routinely observed for iron sulfides grown on steel. The cross-section image in Figure 1 (b) demonstrates that the layer on the pretreated specimen is continuous and is well attached to the surface.

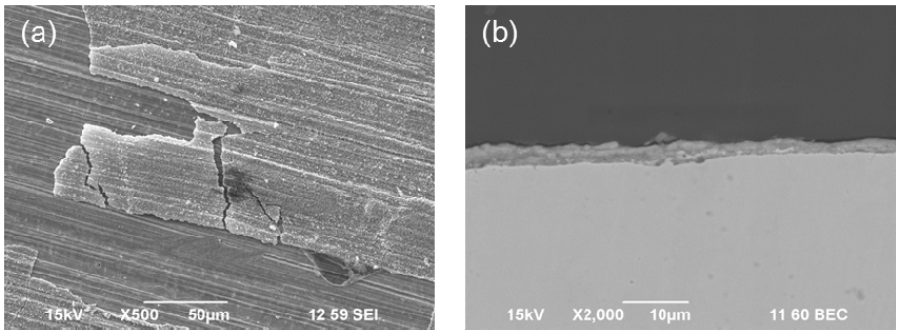

Figure 1. SEM images of representative pretreated steel specimen: (a) Top surface; (b) Cross-section.

Figure 2 shows the XRD pattern of the pretreated specimen. Based on initial peak analysis [50] troilite seemed to be the main component of the layer, however, a more thorough analysis revealed otherwise.

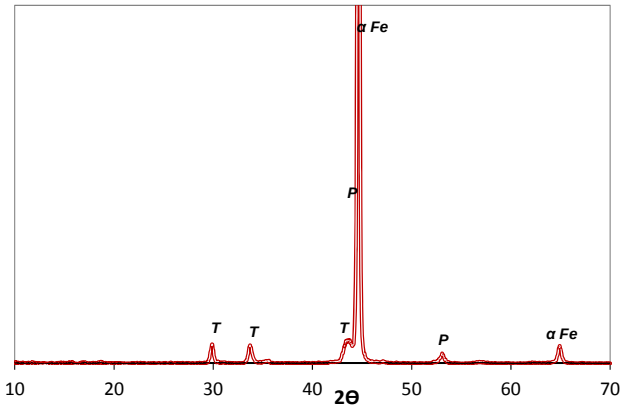

Figure 2. XRD pattern of the pretreated X65 specimens. (P: pyrrhotite, T: troilite).

Part 1- Corrosion of Steel with a Preformed Pyrrhotite Layer Exposed to Aqueous CO_2 Solutions

In aqueous CO_2 corrosion, the pretreated specimen with a pyrrhotite layer was studied under two conditions: in a conductive 1 wt% NaCl electrolyte and a poorly conductive DI water in order to investigate the role of galvanic coupling. However, LPR measurements were not conducted in the experiments without NaCl due to the low solution conductivity. The solution pH which was monitored for the duration of the experiments, was relatively stable (changing from pH 4.0 to pH 4.5).

Figure 3 shows the average corrosion rate of the pretreated specimen exposed to a CO_2 saturated solution with 1 wt% NaCl. This experiment was repeated four times. The average of the measured data is reported with the error bars denoting the maximum and minimum values. The initial corrosion rate was approximately 0.7 mmy^{-1}, compared to the expected bare steel corrosion rate of about 2.0 mmy^{-1} (as calculated using the mechanistic corrosion model described by Zheng, *et al.* [4]). The comparison indicates that the preformed pyrrhotite layer did offer some protection to the steel surface underneath.

However, the initial corrosion rate was not as low as one would expect as a result of a compact and protective layer. When the corrosion rate is controlled by the rate of cathodic reduction then the conductive nature of the pyrrhotite layer should increase the uniform corrosion rate; this can be offset by the same porous layer acting as a diffusion barrier, what should have decreased the corrosion rate. Either way, over a period of three days the corrosion rate decreased to less than 0.1 mmy^{-1}. The specimen OCP increased approximately 20 mV during the experiment.

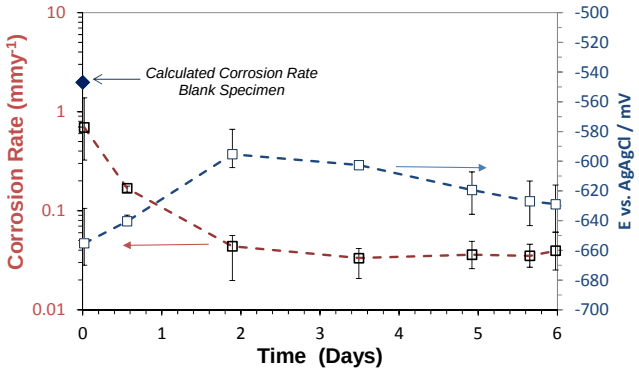

Figure 3. Corrosion rate and OCP of X65 specimen with pyrrhotite type layer vs. time of a sparged solution with 0.097 MPa CO_2 at 30˚C and pH 4.0.

Figure 4 shows the SEM image of the pretreated specimens after exposure to the aqueous CO_2 solutions. Irrespective of the presence of NaCl, the top layers on both images (Figure 4 (a) and Figure 4 (b)) appeared to be similar – with locations where the layer locally collapsed, which were later identified to be points of localized corrosion. Overall, the top layer morphology changed as a result of exposure to the aqueous CO_2 solution as compared to the original surface shown in Figure 1 (a).

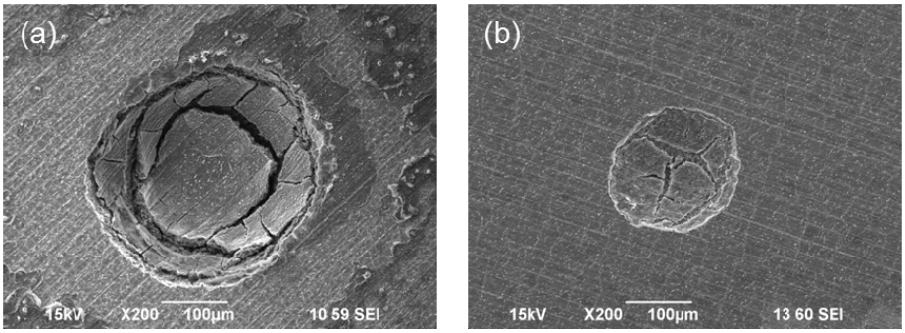

Figure 4. SEM image of pretreated specimens after exposure to an aqueous solution sparged with 0.097 MPa CO_2 at 30˚C and pH 4.0 (a) 1 wt% NaCl, (b) no NaCl.

Figure 5 shows cross-sections of pits formed on the pretreated specimens exposed to the aqueous CO_2 solution with and without NaCl. Small amount of corrosion product was found in the pits, which suggests they were still actively corroding at the time when specimens were retrieved. The area in the vicinity of the pits on both images show that the corrosion product layer was thin, therefore undetectable with XRD.

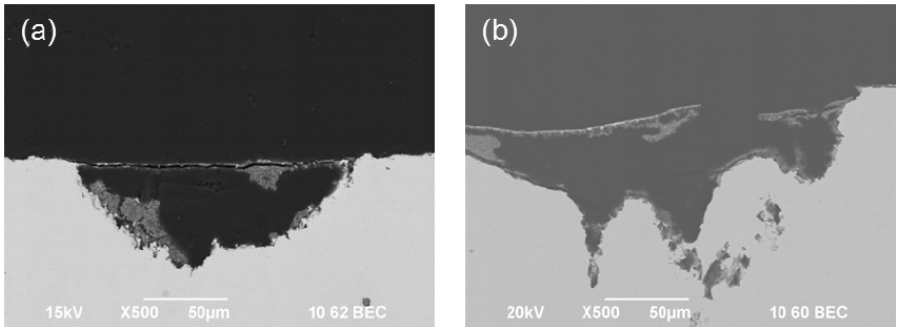

Figure 5. Cross-section image of pretreated specimens after exposure to an aqueous solution sparged with 0.097 MPa CO_2 at 30˚C and pH 4.0 (a) 1 wt% NaCl, (b) no NaCl.

Experimental observation of the pretreated specimens revealed that the preformed pyrrhotite layer underwent dissolution upon its exposure to the aqueous CO_2 solution. Since the preformed layer was not in a thermodynamically stable condition, dissolution of the layer was expected under these test conditions. There have been multiple mechanisms proposed for pyrrhotite dissolution in acidic media.[53–56] One of the reductive mechanisms suggests that H^+ adsorbs onto "anionic sites" on the surface of the pyrrhotite crystals, and this results in a transformation from a nonstoichiometric pyrrhotite to stoichiometric troilite (Reaction 1) with production of H_2S. This is followed by dissolution of troilite to form HS^- and Fe^{2+} shown by Reaction (2).[53–55,57–60]

$$Fe_{1-x}S + 2xe^- + 2xH^+ \rightarrow (1-x)FeS + xH_2S \quad (1)$$

$$(1-x)FeS + 2(1-x)H^+ \rightleftharpoons (1-x)Fe^{2+} + (1-x)H_2S \quad (2)$$

In the current study, it seems that the preformed pyrrhotite layer underwent a dissolution process, which initially started locally and then proceeded to dissolve completely over time. Localized corrosion initiated on these local sites, where the preformed layer dissolved first, leaving a galvanic cell between the exposed steel surface and the remaining pyrrhotite layer. The iron dissolution at the anode is accelerated by an additional cathodic reaction on the surrounding semiconductive pyrrhotite layer.

Pyrrhotite is a semiconductive iron sulfide, which in a conductive solution, forms a galvanic cell when in direct contact with a steel surface. Table 1 shows that pyrrhotite's potential is more positive compared to the steel surface.[39–41] Therefore, the steel surface becomes the anode and corrodes at a higher rate. This galvanic attack is accelerated due to a high cathode/anode surface area ratio, caused by the porous nature of the pyrrhotite layer, which is expected to enhance the rate of H^+ reduction[42].

Figure 6 shows the XRD patterns of the pretreated specimen surface before and after it was exposed for 6 days to the aqueous CO_2 solution. The diffraction patterns indicate that the layer post- exposure was too thin to be detectable by conventional XRD therefore, confirming that the pyrrhotite layer dissolved by the end of the experiment.

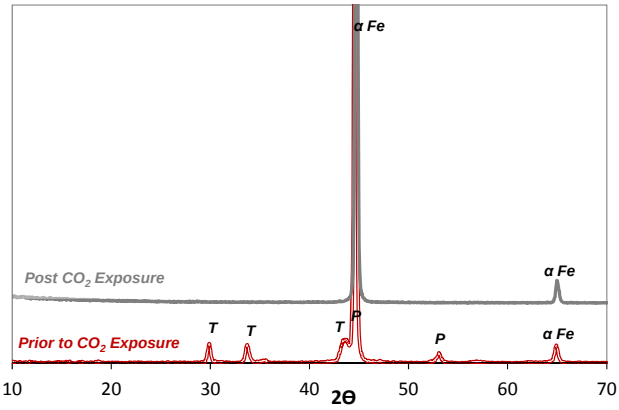

Figure 6. XRD of the pretreated specimen after exposure to an aqueous solution sparged with 0.097 MPa CO_2 at 30˚C and pH 4.0. (P: pyrrhotite, T: troilite).

There seems to be an additional process that took place at the same time. Dissolution of the pyrrhotite layer, produced small amounts of H_2S as described above (Reaction 1), which then reacted with the adjacent steel surface, forming most likely a very thin mackinawite layer. Utilizing XPS analysis, it was shown by Lee, *et al.*[61] that a thin mackinawite layer forms on the surface of a mild steel upon exposure to low concentrations of H_2S, even if it is undetectable by SEM/EDS/XRD. This mackinawite layer probably led to a reduction of the uniform corrosion rate, as shown in Figure 3 (a), but did not affect the localized corrosion.

To confirm the galvanic nature of the observed localized attack, the conductivity of the aqueous solution was varied, which was expected to have a pronounced effect on the magnitude of the galvanic current. To that effect, experiments were conducted in the presence and absence of NaCl. Before the results are presented, it should be noted that in the literature, the role of chloride in localized corrosion is contradictory. [22,28,62–65] While some researchers have attributed localized corrosion initiation of mild steel to the presence of chlorides, work by Fang *et al.*, [22] revealed that the dominant effect is via solution conductivity. Thus, the role of NaCl on localized corrosion in the present study is attributed primarily to its impact on solution conductivity.

Figure 7 shows the SEM images of the pretreated specimens after exposure to solutions with and without NaCl and after the corrosion product layer was chemically removed using a Clarke Solution following the procedure described in ASTM G1 standard[66]. Localized corrosion was observed on both specimens. Profilometry was utilized to measure the depth of the pits and to calculate the time averaged pit penetration rate: PPR= h/t, where h is the deepest pit depth in mm, and t is the time in years. Figure 8 shows the profilometry images, indicating that the specimen exposed to a more conductive solution was attacked at a much higher rate (13.7 mmy^{-1}) than the specimen exposed to the less conductive solution (4.2 mmy^{-1}). Uniform bare steel corrosion rate under these conditions is of the order of 2 to 3 mmy^{-1} making the localized attack propagation in the conductive solution particularly severe, confirming its galvanic nature (see Figure 9).

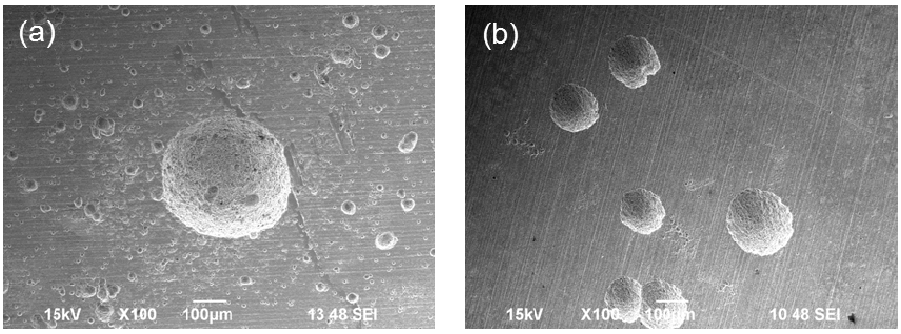

Figure 7. SEM image of pretreated specimens after exposure to an aqueous solution sparged with 0.097 MPa CO_2 at 30˚C and pH 4.0 without corrosion product layer (a) 1 wt.% NaCl, (b) no NaCl.

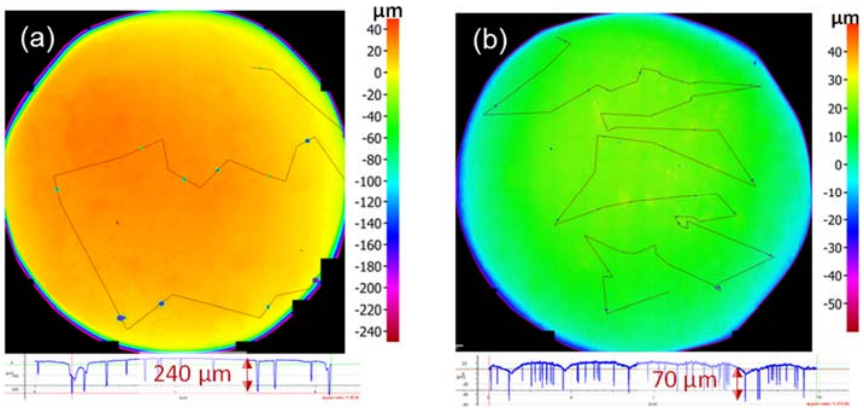

Figure 8. Profilometry image of pretreated specimens after exposure to an aqueous solution sparged with 0.097 MPa CO_2 at 30˚C and pH 4.0 without layer (a) 1 wt.% NaCl, (b) no NaCl.

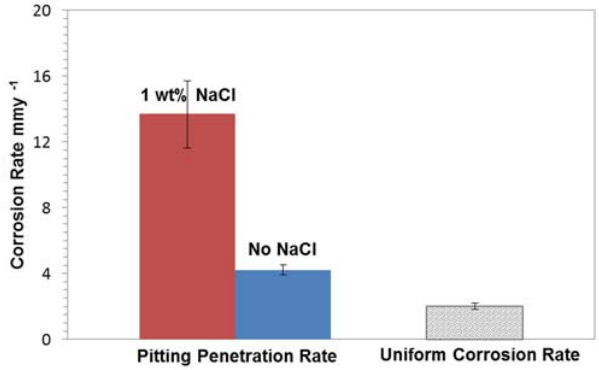

Figure 9. Pit penetration rate of the specimens in an aqueous solution sparged with 0.97 bar CO_2 at 30˚C and pH 4.0.

Part 2- Corrosion of Steel with a Preformed Pyrrhotite Layer Exposed to Aqueous H_2S Solutions

Figure 10 shows the average LPR corrosion rate and the OCP data (from 2 repeated experiments) conducted with the pretreated specimen exposed to an aqueous solution sparged with 0.01 MPa H_2S at two different conditions. The conditions were selected based on the thermodynamic stability of the pyrrhotite layer. In the first condition, the pyrrhotite layer should have been thermodynamically stable (the solution was slightly supersaturated) and was not expected to dissolve (60˚C and pH 6.2 ± 0.1). The second condition (30˚C and pH 4.0 ± 0.1) was selected so that pyrrhotite was not thermodynamically stable (the solution was under-saturated), and it was expected to dissolve. Experiments for each of these two conditions were repeated.

The initial corrosion rate was rather high and similar to that obtained with a bare steel (blank) under the same conditions (as calculated by the mechanistic model described by Zheng *et al.* [2-4]), suggesting that the preformed pyrrhotite layer did not initially offer any appreciable corrosion protection to the steel surface in these conditions. However, the corrosion rate decreased significantly within the first day of exposure to a value close or less than 0.1 mmy^{-1} depending on the experimental conditions (Figure 10 (a)). The OCP change over time (Figure 10 (b)) shows a stable OCP throughout the experiment for the pH 4.0 and 30 ˚C condition, while for the experiment at pH 6.2, 60˚C, OCP increased approximately by 100 mV.

The bulk pH did not change significantly for the case where the pyrrhotite layer was thermodynamically stable and did not dissolve (at pH 6.2). However, when the pyrrhotite layer dissolved, the bulk pH increased from initial pH 4.0 to pH 5.0, bringing it close to saturation for pyrrhotite.

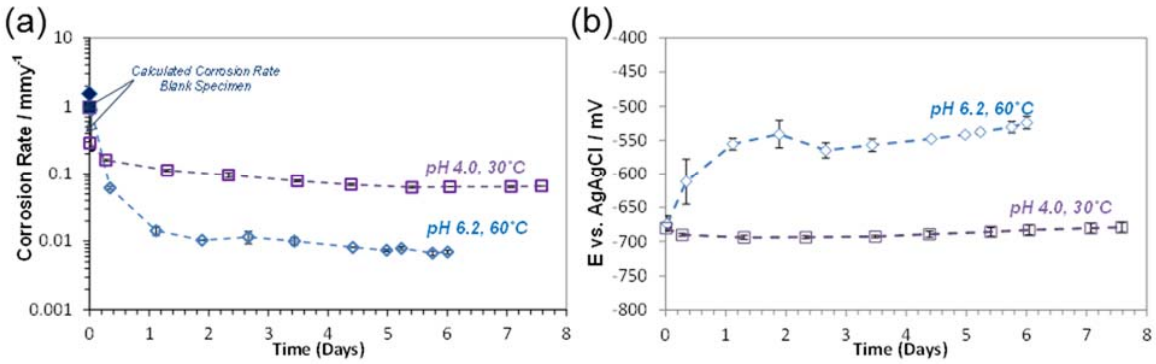

Figure 10. (a) Corrosion rate of pretreated specimen (b) the OCP vs. time in an aqueous solution sparged with 0.01 MPa H_2S in N_2 , 1 wt% NaCl.

Figure 11 shows the SEM images of the specimen at the end of the experiment. It can be observed that the pretreated specimen exposed to the thermodynamically stable condition, was uniformly covered by a corrosion product layer, Figure 11 (a). However, the specimen initially exposed to the under-saturated solution , Figure 11 (b), shows evidence of damage to the initial corrosion product layer as well as a layer below and some precipitation on top. Cross-section analyses were performed to identify the thickness and the morphology of these layers. Figure 12 shows that in both experimental conditions there was a bilayer on the surface. For the specimen exposed to the thermodynamically stable condition, Figure 12 (a), the original pyrrhotite layer seems to be intact (having a similar thickness as that shown in Figure 1 (b)), with an additional layer on top. For the specimen exposed to the under-saturated solution, the final corrosion product layer is much thinner due to pyrrhotite dissolution, Figure 12 (b).

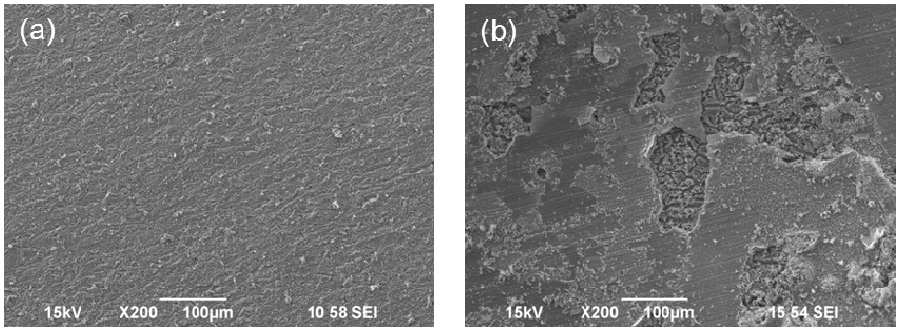

Figure 11. SEM image of pretreated specimens after exposure to an aqueous solution sparged with 0.01 MPa H_2S, 1 wt% NaCl at (a) 60˚C and pH 6.2 (b) 30˚C and pH 4.1.

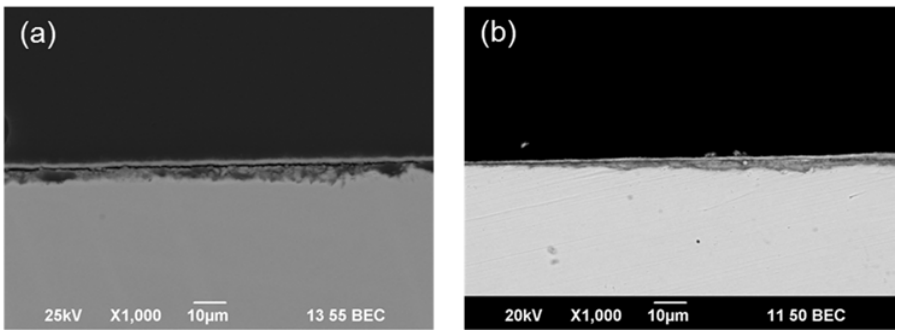

Figure 12. Cross-section image of pretreated specimens after exposure to an aqueous solution sparged with 0.01 MPa H_2S, 1 wt% NaCl at (a) 60˚C and pH 6.2 (b) 30˚C and pH 4.1.

XRD analysis was conducted on specimens after their exposure to the aqueous H_2S solution, in order to characterize the layers and any possible compositional change. Figure 13 shows the XRD patterns of the pretreated specimens before and after exposure to the two experimental conditions. The extra peaks seen on the two exposed specimens were identified to be mackinawite, marked as “M”, and troilite, marked as “T”. The appearance of troilite was expected since the product of a non-stoichiometric pyrrhotite transformation is a stoichiometric troilite (Reaction 1).[54,57,58] Mackinawite has a similar solubility as pyrrhotite and appears to have precipitated. One could wonder why pyrite was not observed on the XRD analysis post H_2S exposure. Less stable iron sulfides usually transform to the more stable iron sulfide polymorphs after longer exposures depending on thermodynamic conditions. In order to form pyrite, much higher pH, higher potentials or higher temperatures are required. The experiments described in the current manuscript were conducted at conditions where pyrite was not thermodynamically stable. Thus, it was not expected to observe any pyrite on the specimens. It is noteworthy that pyrite has a slow kinetics of formation which makes it even more difficult to obtain in laboratory experimentation.

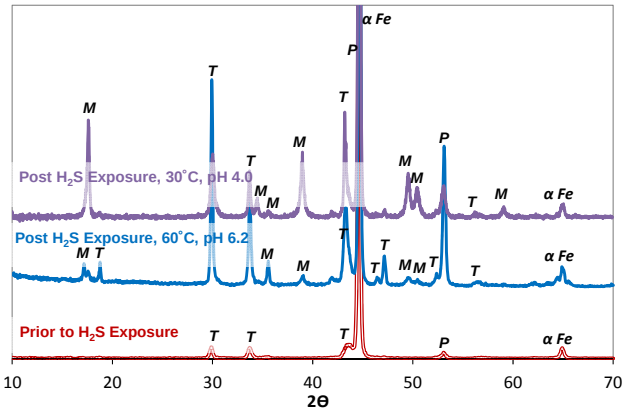

Figure 13. XRD of the pretreated specimens after exposure to an aqueous solution sparged with with 0.01 MPa H_2S at 60˚C and pH 6.2, 30˚C and pH 4.0, 1 wt% NaCl. (P: pyrrhotite, T: troilite, M: mackinawite).

Figure 14 shows the SEM image of the specimens after the corrosion product layer was removed using a Clarke solution[66]. Figure 14 (a) shows a uniformly corroded surface of the specimen exposed to a thermodynamically stable condition, while Figure 14 (b) shows a non-uniform attack of the steel surface of the specimen exposed to the under-saturated solution. However, this non-uniform attack could not be detected in the profilometry image of the same surface shown in Figure 15, which indicates that these areas were rather shallow. In summary, no galvanic localized attack was detected in these experiments, at least not in the same way as was seen in CO_2 experiments reported above.

The cross-section images in Figure 12 show that upon exposure to the aqueous H_2S solution, the preformed pyrrhotite layer was covered with a dense top layer where the pores were most likely filled with the secondary corrosion product layer. Based on XRD analyses, it is most likely that this layer was composed of precipitated mackinawite and possibly troilite/pyrrhotite. It is here hypothesized that this layer, once it formed, has “blocked” the preformed pyrrhotite layer and the steel surface underneath, by limiting the mass transfer of species. Thus, any galvanic cell between the steel surface and the pyrrhotite layer was disrupted and, as a result, localized corrosion propagation was retarded. In the experiment conducted in a supersaturated solution the dense top layer precipitated fast and therefore no localized attack is seen on Figure 14 (a). For the initially under-saturated solution, the dense top layer formed after approximately two days when the bulk solution reached saturation; in the interim the pyrrhotite layer partially dissolved and localized attack was initiated, which was then arrested due to the formation of the dense top layer. This is evidenced by the shallow pits seen in Figure 14 (b).

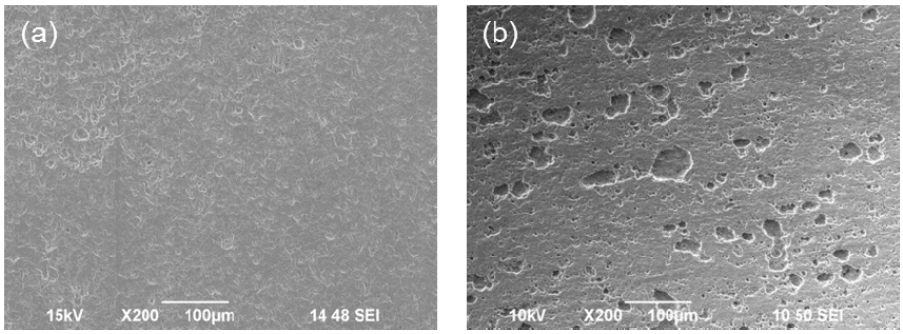

Figure 14. SEM image of the pretreated specimens after exposure to an aqueous solution sparged with 0.01 MPa H_2S, 1 wt% NaCl at (a) 60˚C and pH 6.2, (b) 30˚C and pH 4.0, after removal of the corrosion product layer.

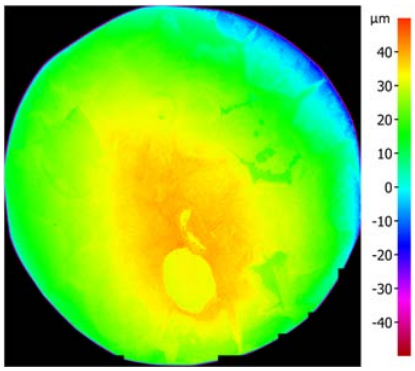

Figure 15. Profilometry image of the pretreated specimen after exposure to an aqueous solution sparged with 0.01 MPa H_2S, 1 wt% NaCl at 30˚C and pH 4.0 without layer.

Part 3- Corrosion of Steel with a Preformed Pyrrhotite Layer Exposed to mixed CO_2/H_2S Solutions

In Part 1 of the present study, it was shown that localized corrosion was observed on pretreated specimens exposed to an aqueous CO_2 solution, due to the uneven dissolution of the pyrrhotite layer which lead to galvanic corrosion. In Part 2, it was shown that in an aqueous H_2S solution, localized corrosion did not take place as a result of a dense layer formation on top of the pyrrhotite layer. It is therefore of interest to investigate the possibility of localized corrosion in mixed CO_2/H_2S environments, which corresponds to more realistic conditions encountered in the field.

As shown in Figure 16 (a), the uniform corrosion rate was higher with CO_2 present than without it, for the same partial pressure of H_2S. The calculated[3–5] bare steel corrosion rate is also shown in Figure 16 (a). The pH in the bulk solution was reasonably stable (± 0.1 pH unit) throughout the experiments with and without CO_2 .

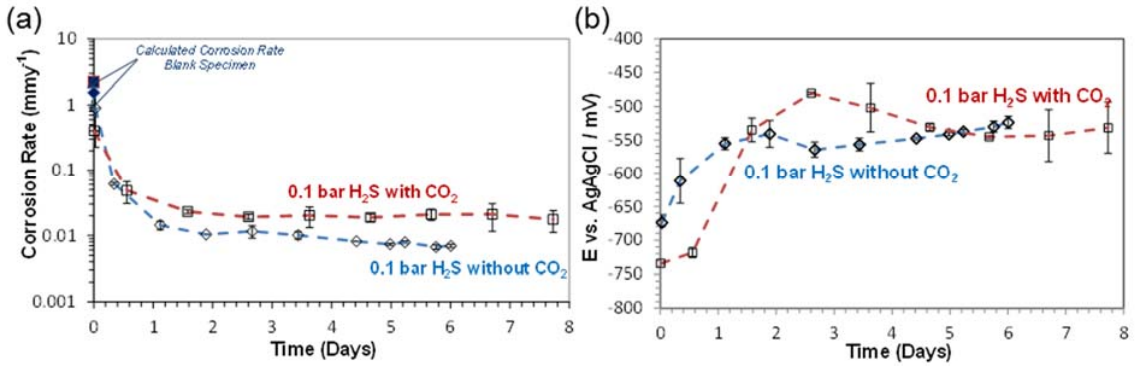

Figure 16. (a) Corrosion rate (b) OCP of pretreated specimen vs. time sparged with 0.01 MPa H_2S with and without 0.07 MPa CO_2, at pH 6.1 and 60˚C, 1 wt% NaCl.

Figure 17 (a) shows the SEM images of the top surface the specimen after the exposure to an H_2S only solution (in the absence of CO_2) where a uniform corrosion product can be seen. A nonuniform appearance of the corrosion product layer is found in the presence of CO_2, Figure 17 (b). If we compare the image in Figure 1 (a) of the pyrrhotite layer before exposure and the image in Figure 17 (b) after exposure to the mixed CO_2/H_2S environment, we can observe the partial transformation of the original pyrrhotite layer.

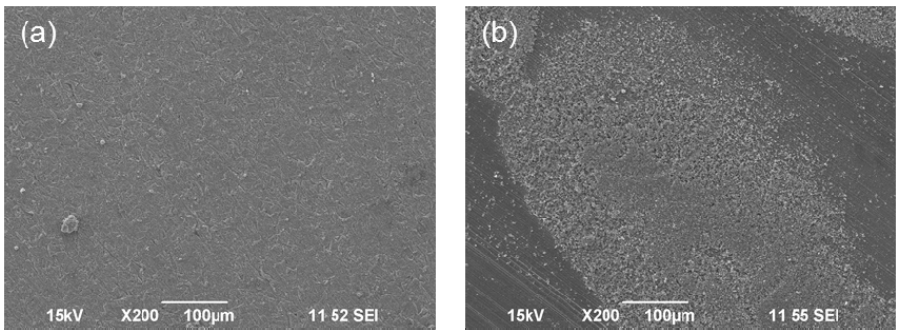

Figure 17. SEM image of pretreated specimens after exposure to an aqueous solution sparged with 0.01 MPa H_2S, 1 wt% NaCl at 60˚C and pH 6.2 (a) no CO_2, (b) 0.07 MPa CO_2.

This is confirmed in Figure 18 (b) where the thinning of the original pyrrhotite layer is obvious. In the absence of CO_2 there is a dense top layer that formed as shown in Figure 18 (a) and also in Figure 12 (a) for a different location. However, this type of layer has not formed in the presence of CO_2 and an appearance of a different "fluffy" phase can be seen. Also, the pyrrhotite layer seems to have been locally detached from the steel surface in the presence of CO_2 which was not the case in the H_2S only environment.

XRD analyses were carried out to determine the composition of the layer on the specimens as the preformed pyrrhotite underwent some transformation in the presence of CO_2. The intensity of the peaks associated with troilite/mackinawite is stronger for the specimen exposed to the H_2S only solution (see Figure 19). It is believed that the "fluffy" phase seen in Figure 17 (b) and Figure 18 (b) is mackinawite.

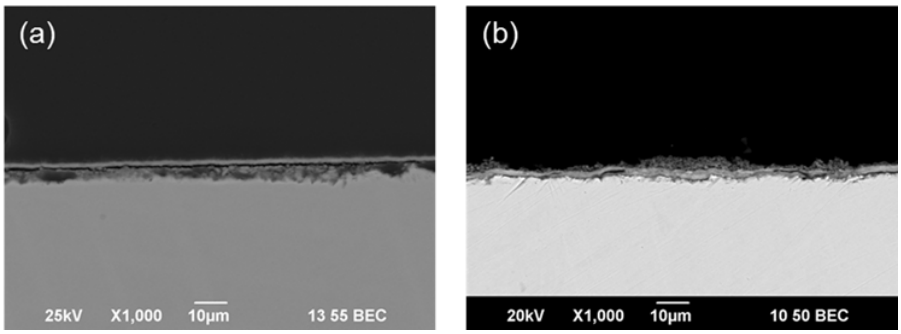

Figure 18. Cross section image of pretreated specimens after exposure to an aqueous solution sparged with 0.01 MPa H_2S, 1 wt% NaCl at 60˚C and pH 6.2 (a) no CO_2, (b) 0.07 MPa CO_2.

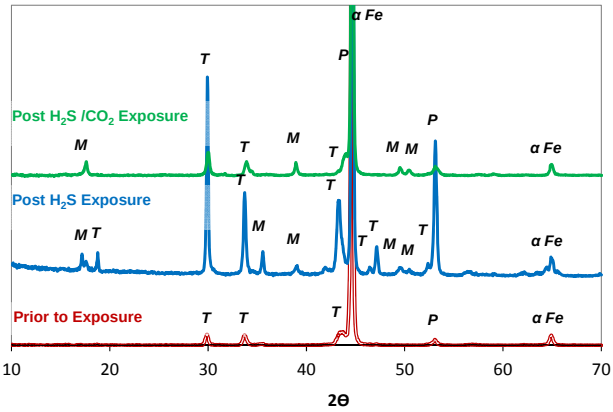

Figure 19. XRD of the pretreated specimens after exposure to an aqueous solution sparged with 0.01 MPa H_2S at 60˚C and pH 6.2 with and without 0.07 MPa CO_2, 1 wt% NaCl. (P: pyrrhotite, T: troilite, M: mackinawite).

Following removal of the layer, Figure 20 (b) shows that the steel surface exposed to the mixed CO_2/H_2S solution underwent localized corrosion, which was not the case in the absence of CO_2 , see Figure 20 (a). This could be explained by the fact that a different layer formed on the specimens upon exposure to different experimental conditions: a dense more protective layer formed in the H_2S only solution and a "fluffy" mackinawite layer formed in the mixed CO_2/H_2S solution.

Profilometry was utilized to measure the depth of the observed pits. Figure 21 shows that the localized attack was found only in one section on the steel surface with the maximum pit depth of 133 m corresponding to 5.5 (±0.5) mmy^{-1} pit penetration rate. It should be noted that these experiments were repeated. In both experiments there were only a few pits concentrated in a limited area.

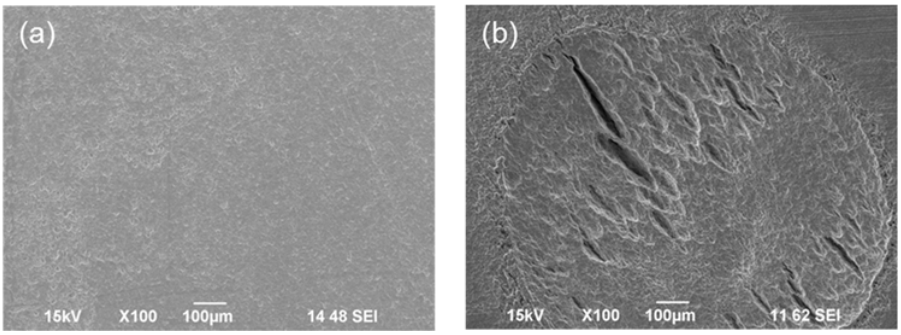

Figure 20. SEM image of the pretreated specimens after exposure to an aqueous solution sparged with 0.01 MPa H_2S, 1 wt% NaCl at 60˚C and pH 6.2, (a) without CO_2, and (b) 0.07 MPa CO_2, after removal of the corrosion product layer.

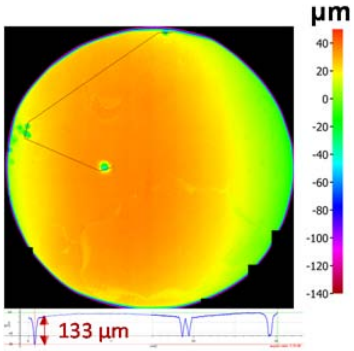

Figure 21. Profilometry image of pretreated specimen after exposure to an aqueous solution sparged with 0.01 MPa H_2S, 0.07 MPa CO_2, 1 wt% NaCl at 60°C and pH 6.2 without layer.

CONCLUSIONS

- ✓ Localized corrosion occurred in an aqueous CO_2 solution with and without NaCl, where the conductive pyrrhotite layer underwent non-uniform dissolution, resulting in partial exposure of the steel surface, leading to initiation of localized attack, which them propagated due to a galvanic coupling between the steel and the remaining pyrrhotite layer.
- ✓ In an aqueous CO_2 solution the presence of 1 wt% NaCl led to a higher solution conductivity, where the localized corrosion rates were found to be approximately three times higher than the localized corrosion rate in the absence of NaCl, which confirmed the galvanic nature of the attack propagation.
- ✓ Localized corrosion was found to a lesser extent in a mixed CO_2/H_2S aqueous solution containing 1 wt% NaCl, where the local dissolution of the pyrrhotite layer was slower and a partially protective mackinawite layer formed.
- ✓ A dense protective layer formed on top of the pyrrhotite layer on the specimen exposed to an aqueous H_2S solution with 1 wt% NaCl. Thus, the preformed pyrrhotite layer dissolution was slowed down significantly, and no localized attack was observed.
- ✓ Overall it is concluded that when a non-uniform semi-conductive pyrrhotite layer is in contact with the steel surface in a corrosive electrolyte, this could lead to galvanically driven localized corrosion.

ACKNOWLEDGMENT

The authors acknowledge the financial support from a joint industry project including BP, Champion Technologies, Chevron, ConocoPhillips, DNV GL, ENI S.p.A., ExxonMobil, Hess, MultiChem, NALCO Energy Services, Occidental Petroleum Co., Petrobras, PETRONAS, PTT, Saudi Aramco, Inpex Corporation, SINOPEC, TOTAL, TransCanada, WGIM, Shell. The authors would like to extend their appreciation to Dr. David Young and Dr. Bert Pots for their advices and contribution for the current study.

REFERENCES

1. S. Nešić, Carbon dioxide corrosion of mild steel (2011), R. Winston Revie, Uhlig's Corrosion Handbook, 3rd ed., Hoboken, NJ, p.229–245.
2. W. Sun, S. Nešić, Corrosion in acid gas solutions (2010), J. A. Richardson, Shreir's Corrosion, 2nd ed., Elsevier, p.1270–1298.

3. Y. Zheng, B. Brown, and S. Nešic, Electrochemical study and modeling of H_2S corrosion of mild steel, Corrosion 70 (2014): p. 351–365.
4. Y. Zheng, J. Ning, B. Brown, S. Nesic, Electrochemical model of mild steel corrosion in a mixed H_2S/CO_2 aqueous environment in the absence of protective corrosion product layers, Corrosion 71 (2015): p. 316–325.
5. Y. Zheng, J. Ning, B. Brown, S. Nesic, Advancement in predictive modeling of mild steel corrosion in CO_2 and H_2S containing environments, Corrosion 72 (2016) : p. 679–691.
6. F. Shi, L. Zhang, J. Yang, M. Lu, J. Ding, H. Li Polymorphous FeS corrosion products of pipeline steel under highly sour conditions, Corros. Eng. Sci. Technol. 102 (2016): p. 1521–1557.
7. J. Ning, Y. Zheng, B. Brown, D. Young, S. Nesic, A thermodynamic model for the prediction of mild steel corrosion products in an aqueous hydrogen sulfide environment, Corrosion 71 (2015): p. 945–960.
8. D.W. Shoesmith, P.Taylor, M.G. Bailey, D.G. Owen, The formation of ferrous monosulfide polymorphs during the corrosion of iron by aqueous hydrogen sulfide at 21˚C, Electrochem. Soc. 127 (1980): p. 1007–1015.
9. L.G. Benning, R. T. Wilkin, H. Barnes, Reaction pathways in the Fe–S system below 100°C, Chem. Geol. 167 (2000): p. 25–51.
10. W.H. Thomason, Formation rates of protective iron sulfide films on mild steel in H_2S-saturated brine as a function of temperature, NACE International CORROSION /78, paper no. 41.
11. F.H. Meyer, O.L. Riggs, R.L. McGlasson, J.D. Sudbury, Corrosion products of mild steel in hydrogen sulfide environments, Corrosion 14 (1957): p. 69–75.
12. Z. Z. W. Zhao, Y. Zou, K. Matsuda, Characterization of the effect of hydrogen sulfide on the corrosion of X80 pipeline steel in saline solution, Corros. Sci. 102 (2016): p. 455–468.
13. D.F. Pridmore, R.T. Shuey, The electrical resistivity of galena, pyrite, and chalcopyrite, Am. Mineral. 61 (1976): p. 248–259.
14. C. I. Pearce, A. D. Pattrick, D. J. Vaughan, Electrical and magnetic properties of sulfides, Rev. Mineral. Geochem. 61(2006): p. 127–180.
15. R. Schieck, A. Hartmann, S. Fiechter, R. Konenkamp, H. Wetzel, Electrical properties of natural and synthetic pyrite (FeS_2) crystals, *J. Mater. Res*. 5 (1990): p. 1567–1572.
16. P.K. Abraitis, R.A.D. Pattrick, D.J. Vaughan, Variations in the compositional, textural and electrical properties of natural pyrite: a review, Int. J. Mine. Process, 74 (2004): p. 41–59.
17. D.J. Vaughan, J.R. Craig, Mineral chemistry of metal sulfides, first ed., Vail-Ballou, New York, 1978, p. 17-117.
18. A.R. Lennie, K.E.R. England, D. Vaughan, Transformation of synthetic mackinawite to hexagonal pyrrhotite: a kinetic study, Am. Mineral. 80 (1995): p. 960–967.
19. K.D. Kwon, K. Refson, S. Bone, R. Qiao, W.L Yang, Z. Liu, G. Sposito, Magnetic ordering in tetragonal FeS: evidence for strong itinerant spin fluctuations, Phys. Rev. B83 (2011): p. 064402_1–064402_7.
20. P.W. Bolmer, Polarization of iron in H_2S-NaHS buffers, Corrosion 21 (1965): p. 69–75.
21. S.P. Ewing, Electrochemical studies of the hydrogen sulfide corrosion mechanism, Corrosion 11 (1955): p. 497–501.
22. H. Fang, Investigation of localized corrosion of carbon steel in H_2S environments, Ph.D. Dissertation, Ohio University, 2012.
23. D.D. MacDonald, B. Roberts, J.B. Hyne, The corrosion of carbon steel by wet elemental sulphur, Corros. Sci. 18 (1978): p. 411–425.
24. G. Schmitt, Effect of elemental sulfur on corrosion in sour gas systems, Corrosion 47 (1999): p. 285–308.
25. N. Yaakob, Top of the Line Corrosion in CO_2/H_2S Environments, Ph.D. Dissertation, Ohio University, 2015.

26. N. Yaakob, F. Farelas, M. Singer, S. Nesic, and D. Young, Localized top of the line corrosion in marginally sour environments, *NACE* International *CORROSION/*2016, paper no. 7695.
27. J. Ning, Y. Zheng, B. Brown, D. Young, S. Nesic, The role of iron sulfide polymorphism in localized H_2S corrosion of mild steel, Corrosion 73 (2017): p. 155–168.
28. J. Kvarekval, G. Svenningsen, Effect of iron sulfide deposits on sour corrosion of carbon steel, *NACE* International *CORROSION*/2016, paper no. 7313.
29. O. Yepez, N. Obeyesekere, and J. Wylde, Study of sour corrosion mechanism under controlled pH, NACE International CORROSION/2016, paper no. 7795.
30. V. Brailovskiy, Effect of pre-exposure of sulfur and iron sulfide on H_2S corrosion at different temperatures, Master of Science, Universitetet i Stavanger, 2011.
31. R.C. Woollam, J.R. Vera, A. Huggins, W.H. Durine, Localized corrosion due to galvanic coupling between FeS-covered and uncovered areas: another oilfield myth?, NACE International CORROSION/2013, paper no. 2715.
32. J. Kvarekval, Corrosion layer breakdown and localized corrosion in CO_2/H_2S environments, *NACE* International *CORROSION*/2012, paper no. 01537.
33. J. Kvarekval, and A. Dugstad, Corrosion mitigation with pH stabilisation in slightlty sour gas/condensate pipelines, *NACE* International *CORROSION*/2006, paper no. 06646.
34. K. Videm and J. Kvarekvål, Corrosion of carbon steel in carbon dioxide-saturated solutions containing small amounts of hydrogen sulfide, Corros. Sci*.* 51 (1995): p. 260–269.
35. J. Kvarekval, R. Nyborg, M. Seiersten, Corrosion product films on carbon steel in semi-sour CO_2/H_2S environments, *NACE* International *CORROSION/* 2002, paper no. 02296.
36. J. Kvarekval, A. Dugstad, M. Seiersten, Localized corrosion on carbon steel in sour glycolic solutions, NACE International CORROSION/2010, paper no. 10277.
37. J. Kvarekval, A. Dugstad, Pitting corrosion in CO_2/H_2S- containing glycol solutions under flowing conditions, NACE International CORROSION/2005, paper no. 05631.
38. J. Amri, J. Kvarekval, and B. Malki, Simulation of solid-state growth of iron sulfides in sour corrosion conditions, NACE International CORROSION/2011, paper no. 11078.
39. C. Almeida, B.F. Giannetti, The electrochemical behavior of pyrite–pyrrhotite mixtures, Electroanal. Chem. 553 (2003): p. 27–34.
40. K.K. Mishro, K. Osseo-Asare, Aspects of the interfacial electrochemistry of semiconductor pyrite (FeS_2), Electrochem. Soc. 135 (1988): p. 2502–2509.
41. L.C. Hamilton, R. Woods, An investigation of surface oxidation of pyrite and pyrrhotite by linear potential sweep voltammetry, Electroanal. Chem. 118 (1981): p. 327–343.
42. D.A. Jones, Principles and prevention of corrosion, second ed.,Prentice-Hall, New Jersey, 1996, p. 168-198.
43. K. Adam, K.A. Natarajan, S.C. Riemer, I. Iwasaki, Electrochemical aspects of grinding media-mineral interaction in sulfide ore grinding, Corrosion 43 (1986): p. 440–447.
44. C. Giovanni, W. Wang, S. Nowak, J.M. Greneche, H. L.ecoq, L. Mouton, M. Giraud, C. Tard, Bioinspired iron sulfide nanoparticles for cheap and long-lived electrocatalytic molecular hydrogen evolution in neutral water, ACS Catal. 4 (2014): p. 681–687.
45. E. Peters, The electrochemistry of sulfide minerals, in: J.O'M. Bockris, D.A.J. Rand and B.J. Welch (Eds.), Trends in electrochemistry, Plenum Press, New York, 1977, pp. 267–290.
46. P.R. Holmes, F.K. Crundwell, Kinetic aspects of galvanic interactions between minerals during dissolution, Hydrometallurgy 39 (1995): p. 353–375.
47. S.N. Esmaeely, B. Brown, S. Nesic, Verification of an electrochemical model for aqueous corrosion of mild steel for H_2S partial pressures up to 0.1 MPa, Corrosion 73 (2017): p. 144–154.
48. P. Jin, W. Robbins, G. Bota, Mechanism of magnetite formation in high temperature corrosion by model naphthenic acids, Corros. Sci. 111 (2016): p. 822–834.

49. P. Jin, S. Nesic, Mechanism of magnetite formation in high temperature naphthenic acid corrosion by crude oil fractions, Corros. Sci. 115 (2017): p. 93–105.
50. Mineralogy Database, http://webmineral.com/, 2016 (accessed 07.02.15).
51. R.G. Arnold, L.E. Reichen, Measurement of the metal content of naturally occurring, metal-deficient, hexagonal pyrrhotite by an x-ray spacing method, Amer. Mineral. 47 (1962): p. 105–111.
52. G.A. Desborough, R.H. Carpenter, Phase relations of pyrrhotite, Econ. Geol. 60 (1965): p. 1431–1450.
53. P. Chirita, and J.D. Rimstidt, Pyrrhotite dissolution in acidic media, Appl. Geochem. 41 (2014): p. 1–10.
54. M.J. Nicol, P.D. Scott, The kinetics and mechanism of the non-oxidative dissolution of some iron sulfides in aqueous acidic solutions, J. S. Afr. I. Min. Metall. (1979): p. 298–305.
55. P.H. Tewari, A.B. Campbell, Dissolution of iron sulfide (troilite) in aqueous sulfuric acid, Phys. Chem. 80 (1976): p. 1844–1848.
56. M.P. Janzen, R.V. Nicholson, J.M. Scharer, Pyrrhotite reaction kinetics reaction rates for oxidation by oxygen ferric iron and for non-oxidative dissolution, Geochim. Cosmochim. Acta 64 (1999): p. 1511–1522.
57. P.H. Tewari, A.B. Campbell, Dissolution of iron during the initial corrosion of carbon steel in aqueous H_2S solutions, Can. J. Chem. 57 (1979): p. 188–196.
58. P.H. Tewari, G. Wallace, A.B. Campbell, The solubility of iron sulfides and their role in mass transport in giroler-sulfide heavy water plants, Research Chemistry Branch, Whiteshell Nuclear Research Establishment (1978): p. 5960.
59. A.V. Kuklinskii, Y.L. Mikhlin, G.L. Pashkov, V.F. Kargin, I.P. Asanov, Conditions for the formation of a nonequilibrium nonstoichiometric layer on pyrrhotite in acid solutions, Russian J. of Electrochem. 37 (2001): p. 1269–1276.
60. J.E. Thomas, W.M. Skinner, R. ST.C. Smart, A mechanism to explain sudden changes in rates and products for pyrrhotite dissolution in acid solution, Geochim. Cosmochim. Acta 65 (2001): p. 1–12.
61. K-L.J. Lee, A Mechanistic Modeling of CO_2 Corrosion of Mild Steel in the Presence of H_2S, Ph.D. Dissertation, Ohio University, 2004.
62. X. Jiang, Y.G. Zheng, D.R. Qu, and W. Ke, Effect of calcium ions on pitting corrosion and inhibition performance in CO_2 corrosion of N80 steel, Corros. Sci. 48 (2006): p. 3091–3108.
63. C.Q. Ren, X. Wang, L. Liu, H.E. Yang, and N. Xian, Lab and field investigations on localized corrosion of casing, Mater. Corros. 63 (2012): p. 168–172.
64. Z.F. Yin, W.Z. Zhao, Y.R. Feng, S.D. Zhu, Characterization of CO_2 corrosion scale in simulated solution with Cl^- ion under turbulent flow conditions, Corros. Eng., Sci. Technol. 44 (2009): p. 453–461.
65. S. Navabzadeh Esmaeely, D. Young, B. Brown, S. Nesic, Effect of incorporation of calcium into iron carbonate protective layers in CO_2 corrosion of mild steel, Corrosion 73 (2017): p. 238–246.
66. ASTM Standard G1, Standard practice for preparing, cleaning, and evaluating corrosion test, Reapproved, 2011.
67. H. Mansoori, R. Mirzaee, F. Esmaeilzadeh, A. Vojood, “Pitting corrosion failure analysis of a wet gas pipeline,” Engineering Analysis 82(2017): p. 16-25.